



Minerva Access is the Institutional Repository of The University of Melbourne

Author/s:

McDougall, SJ;Guo, H;Andresen, MC

Title:

Dedicated C-fibre viscerosensory pathways to central nucleus of the amygdala

Date:

2017-02-01

Citation:

McDougall, S. J., Guo, H. & Andresen, M. C. (2017). Dedicated C-fibre viscerosensory pathways to central nucleus of the amygdala. *Journal of Physiology*, 595 (3), pp.901-917. <https://doi.org/10.1113/JP272898>.

Persistent Link:

<https://hdl.handle.net/11343/291879>

Dedicated C-fiber viscerosensory pathways to central nucleus of the amygdala.

Stuart J. McDougall^{1,2}, Haoyao Guo² and Michael C. Andresen¹

¹Department of Physiology & Pharmacology, Oregon Health & Science University, Portland OR, USA, and ²Florey Institute of Neuroscience and Mental Health, University of Melbourne, Parkville VIC, Australia.

Corresponding author:

Dr. Stuart J. McDougall

Florey Institute of Neuroscience and Mental Health

University of Melbourne, Parkville VIC 3010, Australia

email: stuart.mcdougall@florey.edu.au

Running title: Viscerosensory pathways to the amygdala.

This is the author manuscript accepted for publication and has undergone full peer review but has not been through the copyediting, typesetting, pagination and proofreading process, which may lead to differences between this version and the [Version of Record](#). Please cite this article as [doi: 10.1113/jphysiol.2013.7501](https://doi.org/10.1113/jphysiol.2013.7501).

This article is protected by copyright. All rights reserved.

Keywords:

vagus, solitary, NTS, network, recruitment, afferent

Author Manuscript

Key points

- Emotions are accompanied by concordant changes in visceral function including cardiac output, respiration and digestion. One major forebrain integrator of emotional responses, the amygdala, is thought to rely on embedded visceral afferent information but few details are known.
- Here we retrogradely transported dye from the central nucleus of the amygdala (CeA) to identify CeA-projecting NTS neurons for synaptic characterization and compared them to unlabeled, near-neighbor NTS neurons.
- Solitary tract (ST) afferents converged onto NTS-CeA second-order sensory neurons in greater numbers as well as indirectly via polysynaptic pathways.
- Surprisingly, all mono- and polysynaptic ST afferent pathways to NTS-CeA neurons were organized exclusively as either TRPV1-sensitive or TRPV1-resistant regardless of whether intervening neurons were excitatory or inhibitory.
- This strict sorting provides viscerosensory signals to CeA about visceral conditions as either “normal” via A-fibers or “alarm” via TRPV1 expressing C-fibers and as such this pathway organization likely encodes interoceptive status.

Abstract

Emotional state is impacted by changes in visceral function, including blood pressure, breathing and digestion. A main line of viscerosensory information processing occurs first in the NTS. Here, in rats, we examined the synaptic characteristics of visceral afferent pathways to the central nucleus of the amygdala (CeA) in brainstem slices by recording from retrogradely labeled NTS projection neurons. We simultaneously recorded neuron pairs: one dye positive (i.e. NTS-CeA) and a second unlabeled neighbor. Graded shocks to the solitary tract (ST) always (93%) triggered EPSCs at CeA projecting NTS neurons. Half of the NTS-CeA neurons received at least one primary afferent input (classed 'second order') indicating that viscerosensory information arrives at the CeA conveyed by a pathway involving as few as two synapses. The remaining NTS-CeA neurons received viscerosensory input only via polysynaptic pathways. In contrast, ~3/4 of unlabeled neighboring neurons were directly connected to ST. NTS-CeA neurons received greater numbers of ST related inputs compared to unlabeled NTS neurons indicating that highly convergent viscerosensory signals reach the CeA. Remarkably, despite multi-fiber convergence, all single NTS-CeA neurons received inputs derived from only unmyelinated afferents (TRPV1 expressing C-fibers) or only non-TRPV1 ST afferent inputs – never a combination of both. Such segregation means that visceral afferent information followed separate lines to reach CeA. Their very different physiological activation profiles mean that these parallel visceral afferent pathways encode viscerosensory signals to the amygdala that may provide interoceptive assessments to impact behaviors.

Abbreviations

CAP, capsaicin; CeA, central nucleus of the amygdala; NTS, solitary tract nucleus; ST, solitary tract; TRPV1, transient receptor potential cation channel subfamily V member 1.

Author Manuscript

Introduction

Fear responses increase vigilance and arousal and contain imbedded viscerosensory surveillance of internal organ status (Garfinkel *et al.*, 2014; Klarer *et al.*, 2014; Pena *et al.*, 2014). Although the autonomic components of fear responses are well known, the underlying mechanisms, structure and organization of visceral afferent contributions responsible for coordinated, emotion-appropriate visceral states are less clear (Parsons & Ressler, 2013; Garfinkel & Critchley, 2016). The amygdaloid complex deep within the mid-temporal lobe is a key integrative center for emotional processing of cognitive and visceral information (LeDoux, 2000; Maren & Quirk, 2004). Intense anatomical interconnections link the amygdala with cortical structures but the central nucleus of the amygdala (CeA) is most closely associated with neurohumoral and brainstem autonomic aspects of conditioned fear responses (Sah *et al.*, 2003; Ulrich-Lai & Herman, 2009). The CeA critically orchestrates shifts in visceral homeostatic states via efferent projections to the brainstem at the periaqueductal gray, parabrachial nucleus and the nucleus of the solitary tract (NTS) and may help to distinguish between 'physiological' and 'psychological' stressors (Dayas *et al.*, 2001; Ulrich-Lai & Herman, 2009).

Primary afferents of the VII, IX and X cranial nerves convey the physiological status of visceral conditions routed along their solitary tract (ST) axons to the ST nucleus (NTS) (Andresen & Kunze, 1994). NTS neurons include reciprocal connections to and from specific CNS regions including the amygdala (Loewy, 1990; Saper, 2002; Travagli *et al.*, 2006), but little is known about the nature of the functional connections. Viscerosensory afferent excitation results in activation of NTS projection neurons that directly target the CeA (Ricardo & Koh, 1978; Danielsen *et al.*, 1989; Kapp *et al.*, 1989; Geerling & Loewy, 2006).

This NTS to CeA pathway impacts behavioral responses ranging from stress to satiety (Williams *et al.*, 1998; Viltart *et al.*, 2006). Viscerosensory information arrives via two broad phenotypic classes of afferents: the majority via C-fiber primary afferent axons and the remainder along myelinated afferents. The C-fiber cranial afferent neurons express TRPV1, generally have high physiological activation thresholds and are often silent in normal conditions (Andresen *et al.*, 2012). Thus as a group, C-fibers are generally most active in supra-physiological states of visceral function common in pathophysiology. A-fibers generally lack TRPV1 and their low thresholds and high sensitivity mean that they are often quite active normally even during resting or basal conditions (Andresen *et al.*, 2012). Despite this dichotomy, very little is known about the organization and qualities of information processing and flow beyond NTS to other brain destinations. We hypothesized that the direct NTS-CeA pathway would be driven by convergent C-fiber afferents. Here we aimed to characterize cranial afferent inputs, their fiber type and connecting pathways to NTS neurons that project to the CeA.

Surprisingly, our results indicate that cranial afferent information to the CeA follows two separated pathways segregated by the originating TRPV1-based afferent phenotype. Incorporating well established differences in the physiological discharge characteristics of these phenotypic classes, this segregation means that the pathway lacking TRPV1 delivers information reporting largely resting/basal physiological conditions. Whereas the TRPV1+ C-fiber pathway signals primarily during extraordinary visceral circumstances that are common during stress or in pathophysiological states. This organization of segregated interoceptive afferent information likely helps to shape central integration at CeA during autonomic and stress-like behaviors.

Author Manuscript

Methods

Ethical approval

All animal procedures were performed with the approval of the Institutional Animal Care and Use Committee at Oregon Health & Science University and conform to the guidelines of the National Institutes of Health publication "Guide for the Care and Use of Laboratory Animals", and in accordance with the Prevention of Cruelty to Animals Act 1986 under the guidelines of the National Health and Medical Research Council Code of Practice for the Care and Use of Animals for Experimental Purposes in Australia and approved by the Animal Ethics Committee at the Florey Institute of Neuroscience and Mental Health.

Amygdala injections - retrograde tracer.

Adult Sprague Dawley male rats (Charles River Laboratories, Inc., Wilmington, MA and the Florey Core Animal Services) (161 ± 7 g, $n = 64$) were anesthetized (ketamine 60 mg/kg, xylazine 6 mg/kg, acepromazine 1 mg/kg; i.p. at OHSU or 5% induction and 1.5-2% maintenance isoflurane at Florey). Anesthesia level was confirmed by the absence of both the flexor withdrawal and corneal reflex. In a stereotaxic procedure to inject Retrobeads™ (100 nl, Red IX, Lumafluor Inc.), rats were placed in a stereotaxic frame and an incision made to gain access to the skull, holes were hand drilled through the skull over the target sites and the dura mater pierced. A glass pipette was lowered into the brain and retrograde tracer injected into the CeA cell column within co-ordinates ranging from -2.0 to -2.3 AP, 4.0 to 4.22 ML and -8.9 to 8.6 DV to produce injection sites from -1.88 to -3.3 mm AP of bregma. The pipette was removed, skin sutured and Meloxicam (1 mg/kg, s.c.) administered. Rats were housed individually with standard rat chow and water *ad libitum* and monitored (including body weight measurements) daily for 7 days after stereotaxic surgery and weekly

thereafter. Rats recovered for a minimum of 10 days (26 ± 2 days) before slice electrophysiology experiments were carried out. Following removal of the brainstem (see below), the forebrains were sectioned ($200\ \mu\text{m}$) and injection sites photographed on the day of electrophysiology experiments for compilation with NTS neuron labeling in relation to dye location in the amygdala (Figure 1).

Brainstem slice preparation.

Horizontal brainstem slices were prepared as described previously (Doyle & Andresen, 2001) and used to study the amygdala tracer injected rats. Briefly, adult rats (344 ± 11 g) were deeply anesthetized with isoflurane (5%) and the brainstem removed 10-30 days following amygdala tracer injection. Anesthesia level was confirmed by the absence of the flexor withdrawal reflex and the chest compressed to stop the heart, the spinal cord severed at C1 and skull bones removed to access and remove the brain stem. The medulla was rapidly cooled and trimmed rostral and caudal to yield a brainstem block centered on obex. A rostral-caudal wedge of ventral brainstem was removed in order to orient the remaining tissue to yield a single, $250\ \mu\text{m}$ thick, horizontal slice which contained the greatest length of ST axons together with the medial NTS. Slices were cut with a sapphire knife (Delaware Diamond Knives, Wilmington, DE) mounted in a vibrating microtome (VT1000S; Leica Microsystems Inc., Bannockburn, IL). The external solution was an artificial cerebrospinal fluid (ACSF) containing (mM): 125 NaCl, 3 KCl, 1.2 KH_2PO_4 , 1.2 MgSO_4 , 25 NaHCO_3 , 10 dextrose and 2 CaCl_2 . Slices were secured with a nylon mesh in a tissue chamber and perfused with ACSF at 34°C , 300 mOsm, bubbled with 95% O_2 -5% CO_2 .

NTS-CeA neuron quantification and correlation with injection site.

The first phase of working with each slice began with a survey and count of the total number of retrogradely labeled fluorescent cell bodies within the single horizontal slice containing NTS. This survey work was performed using the 40X objective together with the appropriate filter set and all NTS subnuclei were checked. The tallies in each slice is registered in grayscale and overlaid at the corresponding dye injection sites within the amygdala (Figure 1). Once this procedure was completed then paired patch recording commenced.

Paired whole cell recordings.

Recording pipettes (2.8 – 4.2 M Ω) were guided by fluorescent label localized to neurons in the caudal NTS using anatomical landmarks (Figure 2). Neurons were visualized (Doyle *et al.*, 2004) using infrared illumination with differential interference contrast optics (40X water immersion lens) and filter set 15 with mercury lamp on an Axioskop-2 FS plus fixed stage microscope (Zeiss, Thornwood, NJ) with digital camera (Hamamatsu Photonic Systems, Bridgewater, NJ). Paired recordings were attempted in most slices, where neighboring, unlabeled neurons were selected near to dye positive cells for simultaneous recordings. Results from a total of 22 successful neuron pairs (NTS-CeA with near neighbor unlabeled) are reported here (Figure 2). Pipettes were filled with a low Cl⁻ intracellular solution containing (mM): 6 NaCl, 4 NaOH, 130 K-gluconate, 11 EGTA, 1 CaCl₂, 1 MgCl₂, 10 HEPES, 2 Na₂ATP, and 0.2 Na₂GTP (pH 7.3 and 290 mOsm). As a consequence $E_{Cl} = -69$ mV, IPSCs had small amplitudes at $V_H = -60$ mV, though more prominent outward current amplitudes were achieved by shifting to $V_H = -40$ mV in some cases. All recordings were made in open, whole cell patch configuration under voltage clamp using a Multiclamp 700B (Molecular Devices, Sunnyvale, CA). Signals were sampled at 20 kHz and filtered at 10 kHz

using p-Clamp software (version 10.2, Molecular Devices, Sunnyvale, CA). Reported voltages were corrected for the calculated liquid junction potential (-10.7 mV at 34 °C).

ST shock intensity-recruitment profiles

The concentric bipolar stimulating electrode (200 μm outer diameter; Frederick Haer Co., Bowdoinham, ME) was placed on the visible ST approximately 1–3 mm rostral from recorded neuron cell bodies (Figure 2). Minimal stimulus-intensity protocols with incremental recruitment define discrete inputs to central neurons (Allen & Stevens, 1994; Rancz *et al.*, 2007), where delivery of shocks to activate afferents distant from the recorded cells produced discrete, unitary recruitment-intensity profiles (Blitz & Regehr, 2005; Acuna-Goycolea *et al.*, 2008). Thus, passing current via the stimulating electrode activated ST primary afferents to trigger postsynaptic currents (PSCs). The remote placement of the electrode minimized the likelihood that electrical shocks would activate non-ST axons or local neurons (Doyle & Andresen, 2001; Doyle *et al.*, 2004; Bailey *et al.*, 2008). Once stable recordings of each neuron were established a series of test shocks graded in intensity were delivered to the ST. A finely graded synaptic recruitment routine (see MPEG detailed sequence) uncovered contributions of convergent individual inputs (McDougall *et al.*, 2009). Individual inputs were discriminated on the basis of their characteristic latency, waveform and recruitment threshold. Multiple trials together with re-testing of some ST shock intensities indicated that these critical values were important to the characteristics of each input resulting in the recorded PSC. A Master-8 isolated programmable stimulator (A.M.P.I., Jerusalem, Israel) generated single shocks as well as bursts of five ST shocks at 50 Hz every 6 s (shock duration 0.1 ms) for a minimum of 10 consecutive sweeps for each shock intensity trial. All neurons were tested with stimulus shock intensities from 0 to 1000 μA .

From 0 to 100 μA , step changes were 10 μA (minimum) and from 100 to 1000 μA , step changes were 100 μA (minimum). The order of shock intensity presentation varied. Inhibitory PSCs (IPSCs) were often recognized by their prolonged decaying phase and to improve signal to noise ratios, the holding current was shifted to -40 mV to take advantage of an increased Cl^- driving force and shocks repeated. Plots of the event amplitudes (discriminated by arrival time and waveform) against stimulus intensity created stimulus recruitment profiles to compare across events and allows quantification of afferent input. The stimulus recruitment profile of each synaptic event at minimum intensity is considered to reflect the all-or-none axon activation characteristics of the ST fiber initiating the recorded EPSC or IPSC.

Discriminating mono- from polysynaptic and TRPV1+ from TRPV1- ST synaptic responses.

Synaptic latency jitter and failure rates were considered reliable indices that distinguished direct contacts from ST afferents (monosynaptic) from indirect (polysynaptic) afferent pathways to NTS neurons. Analysis of latency was based on the responses to the first shock in the train of five (PSC_1). Shock to shock variability in latency, synaptic jitter, for PSC_1 was calculated >30 events as the standard deviation (SD) of latency and served as a critical indicator of synaptic order. PSC_1 jitters of <200 μs were considered monosynaptic but jitters >200 μs indicated a polysynaptic connection from the ST (Doyle & Andresen, 2001; Bailey *et al.*, 2006). This synaptic jitter criterion matches the jitter characteristics of dye-identified second order NTS neurons using anterogradely transported label from the aortic depressor nerve (Andresen & Peters, 2008). As expected, polysynaptic pathways activated by ST shocks were particularly prone to synaptic failures even with infrequent stimuli (Bailey *et al.*, 2006; Andresen & Peters, 2008). Suprathreshold ST shocks that evoked no identifiable PSC

within the latency time window characteristic of that PSC were counted as synaptic failures and failure rates were calculated for PSC₁ over 40 trials as a percent of total ST shocks delivered at a constant, supra-threshold intensity. Neurons that received at least one excitatory monosynaptic input were defined as second order NTS neurons. Neurons which received only polysynaptic inputs to ST shocks were classified as higher order NTS neurons. Neurons that exhibited no ST-evoked synaptic responses to high intensity shocks (up to 1000 μ A) were considered “not connected” to ST afferents but are included in compiled population totals. The final step in the synaptic interrogation was to expose slices to a continuous infusion of the TRPV1 agonist capsaicin (CAP) initially dissolved in ethanol and diluted with ACSF to 100 nM. CAP blockade of ST-evoked synaptic events classified the initiating primary ST afferent as TRPV1+. The mechanism of CAP-selective block appears to be depolarization of voltage dependent excitability in the ST afferent axons which interrupts transmission from afferents expressing TRPV1 (Hofmann & Andresen, 2016).

Data and Statistics Analysis.

ST evoked PSC amplitudes were based on 40 ‘successful’ iterative evoked events for each input. However, in neurons receiving converging inputs, compound synaptic events were excluded from amplitude analysis despite their use in enumerating distinct inputs. Thus we restricted this analysis to the minimal evoked response or those events sufficiently separated in onsets. Therefore, 60 of 138 input amplitudes in NTS-CeA and 15 of 42 input amplitudes in unlabeled NTS neurons were excluded from the overall means reported in the results. Failure rates were calculated from a minimum of 40 ST test shocks. Input variables including latency, jitter, amplitude and failure rates for PSC₁ were not normally distributed and thus were compared between groups by rank values using a Kruskal-Wallis, one-way ANOVA on

ranks with a Dunn's post hoc test. Proportion data sets were compared using a one tail z-test and input convergence rates by one way ANOVA (SigmaStat, San Jose, CA). All data are reported as mean \pm SEM, $p > 0.05$ was defined as statistically significant.

Author Manuscript

Results

NTS-amygdala neurons project ipsilaterally to CeA.

Stereotaxically directed injections resulted in dye deposited along the rostral-caudal extent but generally within the subnuclear borders of CeA (Figure 1). To gauge the connections between injection sites in CeA ($n = 64$) and the yield of labeled neurons in medial NTS, we mapped the location of dye injections and then registered the dye profile in a gray scale depiction of the number of fluorescence positive NTS neurons counted in corresponding slices (Figure 1). Such yields ranged between zero and 26 neurons per injection in a single 250 μm corresponding NTS slice. All horizontal brainstem slices were inspected for labeled neurons in the contralateral medial NTS, ipsilateral lateral NTS, ipsilateral rostral NTS and finally ipsilateral medial NTS. We could not observe the entire commissural NTS due to the tilted slice orientation needed to preserve ST axons connected with NTS neurons. The fluorescently labeled cell bodies of these NTS-CeA projection neurons were found broadly distributed only ipsilaterally within the medial portions of NTS (Figure 2). Cell bodies were robustly labeled but were generally isolated with few adjacent NTS cells bearing retrograde dye (Figure 2A). No retrogradely labeled NTS-CeA neurons were found lateral to the ST or contralateral across the midline (Figure 2B). Generally, injections made in the mid-region of the CeA, from -2.2 to -2.56 mm relative to bregma, yielded the greatest numbers of labeled neurons in NTS. This pattern of injection sites indicated that the central arbors of NTS-CeA projection neurons were concentrated in the CeA division of the amygdala. Off-center injections, i.e. dye deposits which only partially overlapped with the borders of CeA, resulted in fewer retrogradely labeled NTS neurons. Dye injections that did not overlap CeA failed to label any neurons in NTS ($n=4$ rats) suggesting that NTS neurons primarily project to the central rather than the lateral or basolateral subnuclei. These retrograde tracer findings suggest that NTS-CeA projection neurons were broadly distributed in caudal portions of

medial NTS and these neurons projected to the CeA with little evidence of contacting neighboring subnuclei of the amygdala. Next we determined whether such neurons could be activated by ST afferent pathways.

Graded ST afferent activation identifies multiple synaptic inputs.

Single horizontal brainstem slices were assayed electrophysiologically from each animal. Under fluorescence illumination, dye positive cell bodies (NTS-CeA neurons) were approached with a patch pipette for recording (Figure 2A). A second nearby neuron which was dye negative (unlabeled) was recorded with a second pipette. Once both neurons were ready for study, shocks were delivered to the ipsilateral ST and repeated every 6 s (0.17 Hz) – an interval which produces stable responses over extended periods (Peters *et al.*, 2010). The shock intensity was gradually increased until a ST-synchronized synaptic event was successfully activated in either neuron (Figure 3). The graded intensity recruitment process was repeated with progressively higher and/or lower shock intensities to best characterize the inputs until no further changes occurred in the response (see Supporting Information; supplementary video and instruction file). Each newly recruited synaptic event had a unique shock intensity threshold beyond which that event did not change in latency, shape or amplitude, i.e. all non-compound events were all-or-none and spontaneous events not synchronized to the ST shock were ignored in this analysis. In no case, did we detect evidence in the recruitment protocols for synaptic events that were of common ST origin in paired neighboring neurons, i.e. synaptic events activated in both neurons with an identical threshold intensity consistent with activation of a single ST primary afferent diverging to two target neurons (McDougall & Andresen, 2013). High intensity ST shocks failed to evoke responses in 4 NTS-CeA neurons and 2 unlabeled neighboring NTS cells. These numbers of

“unconnected” neurons were similar or lower than commonly encountered in previous NTS preparations and these cells were not studied further but are considered in population comparisons. Given the thin slices studied, the following reports of our synaptic studies likely underestimate the total numbers of NTS-CeA neurons that exist in the intact system.

NTS-CeA second order sensory neurons receive multiple primary afferent inputs.

Increasing the ST stimulus intensity activated first one and then often multiple unique EPSCs in individual NTS-CeA neurons (Figure 3A). The consistent waveform and minimal shock-to-shock variation in the latency (jitter = SD of latency) indicated that many evoked EPSCs were monosynaptic unitary responses to ST afferent activation (Doyle & Andresen, 2001) and thus such neurons were identified as second order sensory neurons. Recruitment profiles for NTS-CeA second-order sensory neurons most commonly showed multiple convergent ST-evoked EPSCs with unique thresholds and distinct latencies and waveforms (Figure 3A & A₁). Single, high intensity shocks activated multiple ST axons and generated complex compound events that directly converged on single NTS-CeA second-order sensory neurons. Such compound events from strong ST shocks often obscured, smaller events that were so clearly delineated with weaker shocks. The onset of the initial event in the compound EPSCs could be used to calculate latencies and these met the monosynaptic criterion (<200 μs). The jitter values were unique across EPSC subcomponents and reflect variations in glutamate release from the underlying individual ST afferents (Figure 3A₂). Recruitment thresholds were defined across multiple trials at the same shock intensity, and these monosynaptic EPSCs rarely if ever failed (Figure 3A₃, right). Combined, these findings indicate primary afferent inputs converging on single NTS-CeA second-order sensory neurons. Unlabeled neurons generally received inputs that met monosynaptic jitter criteria,

where most often even high intensity ($> 500 \mu\text{A}$) ST shocks recruited only a single, low jitter EPSCs (Figure 3B). Thus, recruitment profiles in such neurons neighboring NTS-CeA neurons were simple for these unfailing EPSCs (Figure 3B₃). For these unlabeled second order NTS neurons, EPSC amplitudes and onsets were very consistent and jitters were $<200 \mu\text{s}$ (Figure 3B). There were no differences between NTS-CeA and neighboring unlabeled neurons with respect to mean monosynaptic EPSC characteristics; latencies ($4.4\pm 0.2 \text{ ms}$ vs $4.9\pm 0.4 \text{ ms}$); jitter ($137\pm 6 \mu\text{s}$ vs $127\pm 9 \mu\text{s}$); amplitudes ($n=22$ inputs, $107\pm 18 \text{ pA}$ vs $n=15$ inputs, $104\pm 12 \text{ pA}$); and failures ($2\pm 1\%$ vs $3\pm 2\%$) ($p>0.05$, one-way ANOVA). Thus as expected, ST primary afferent transmitter release properties are similar across second order NTS neurons irrespective of their target.

ST shocks also activate polysynaptic inputs to NTS-CeA second order sensory neurons.

In many NTS-CeA second-order sensory neurons, ST synaptic responses with highly variable latencies (jitter $>200 \mu\text{s}$) could also be recruited and produced much more complex synaptic patterns (Figure 4A). The high jitter of these synaptic events indicated that the input path to these neurons followed an indirect, therefore multi-neuronal or polysynaptic pathway from ST initiation. In some cases, these events were generated by intervening inhibitory interneurons activated by primary (ST) afferents and all had high jitter. In the case of ST-evoked IPSCs, shifting the recording to a depolarized holding potential ($V_{\text{H}} = -40 \text{ mV}$) produced outward synaptic currents that were difficult to discern at $V_{\text{H}} = -60 \text{ mV}$ (Figure 4A, left-most panels). Polysynaptic EPSCs could also be evoked in some neurons by ST shocks. However, there was no relationship between the absolute ST test shock intensity and the excitatory or inhibitory nature of the synaptic event, i.e. the lowest intensity shocks in some neurons activated polysynaptic IPSCs and greater intensity shocks added monosynaptic

EPSCs (e.g. Figure 4). As expected for directly linked ST-EPSCs, synaptic failures were generally near zero but polysynaptic events failed quite often, even across multiple ST-evoked PSCs that were well separated in time (Figure 4 D, right). Such mixed synaptic responses (mono- with poly-synaptic EPSCs and/or IPSCs) were common in NTS-CeA second order sensory neurons and indicated that such neurons received convergent information directly and indirectly from primary afferent activation. Note that even in single second order neurons with highly complicated synaptic mixtures, the combination of graded ST intensity and multi-trial testing reliably and reproducibly identified multiple distinct mono- and polysynaptic EPSC-IPSC combinations (Figure 4). We found that mean polysynaptic EPSC characteristics were similar ($p > 0.05$, one-way ANOVA) across second order neurons: NTS-CeA (32 inputs across 20 neurons) and paired unlabeled neurons (12 inputs across 8 neurons); latencies (6.5 ± 0.4 ms vs 6.3 ± 0.6 ms); jitter (373 ± 36 μ s vs 499 ± 91 μ s); amplitudes ($n=16$ EPSCs, 59 ± 9 pA vs $n=6$ inputs, 60 ± 14 pA); and failures ($21 \pm 3\%$ vs $40 \pm 8\%$). Overall, the characteristics of polysynaptic IPSCs in NTS-CeA second-order sensory neurons (6 IPSCs across 6 neurons) were similar ($p > 0.05$, one-way ANOVA) to paired unlabeled second order neurons (2 IPSCs across 2 neurons) with similar latencies (8.5 ± 1.5 ms vs 8.1 ± 0.2 ms); jitter (633 ± 172 μ s vs 603 ± 340 μ s); amplitudes ($n=5$ IPSCs, 36 ± 7 pA vs $n=1$ input, 37 pA); and failure rates ($37 \pm 12\%$ vs $49 \pm 29\%$).

NTS-CeA neurons are commonly higher order sensory neurons.

Not all dye-labeled NTS neurons responded to ST shocks with low jitter synaptic events (Figure 5), but rather, ST shocks activated multiple, high jitter responses consistent with convergence of several ST activated, polysynaptic pathways onto these single neurons. The synaptic responses recorded in these NTS-CeA higher order sensory neurons were often

complex with multiple synaptic failures and variable amplitudes that took the form of EPSCs or IPSCs (Figure 5). EPSCs were inward current synaptic events with fast kinetic waveforms (Figure 5A). However, we also observed IPSCs with slower kinetics and small amplitudes at $V_H = -60$ mV (Figure 5B) that became accentuated, outward currents by shifting V_H more positive to E_{Cl} . ST evoked IPSCs exhibited characteristically slow, long lasting kinetics, high jitter and frequent failures. In two neurons, high intensity ST shocks activated low jitter monosynaptic IPSCs consistent with a spreading stimulus which directly activated inhibitory interneurons (McDougall & Andresen, 2012b) and were excluded from group analysis. ST derived IPSCs were much less common than ST evoked mono or polysynaptic EPSCs in NTS-CeA neurons. However, increasing the ST shock intensity often recruited additional excitatory synaptic currents which often obscured IPSCs so this approach likely underestimates both the number and characteristics of additional ST-derived inhibitory inputs. Polysynaptic EPSC mean characteristics were similar ($p > 0.05$, one-way ANOVA) between NTS-CeA (35 inputs across 22 neurons) and paired unlabeled higher order neurons (5 inputs across 3 neurons); latencies (7.2 ± 0.5 ms vs 5.5 ± 0.7 ms); jitter (437 ± 41 μ s vs 493 ± 121 μ s); amplitude ($n=27$ inputs, 47 ± 6 pA vs $n=3$ inputs, 62 ± 27 pA); and failures ($28 \pm 4\%$ vs $33 \pm 9\%$). Likewise, polysynaptic IPSC characteristics between NTS-CeA (14 inputs across 10 neurons) and paired unlabeled higher order neurons (2 inputs across 2 neurons) were also similar; latencies (8.9 ± 0.5 ms vs 6.0 ± 0.4 ms); jitter (669 ± 157 μ s vs 647 ± 88 μ s); amplitude (no compound measurements, thus $n=8$ inputs, 30 ± 5 pA vs $n=2$ inputs, 44 ± 7 pA); and failures ($43 \pm 7\%$ vs $34 \pm 11\%$) ($p > 0.05$, one-way ANOVA). Thus, higher order NTS neurons whether projecting to CeA or not received inputs from interneurons that had generally similar synaptic characteristics.

NTS-CeA neurons are highly integrative.

In aggregate, proportionally fewer NTS neurons that project to CeA were second order (n = 29 of 58) compared to the population of neighboring unlabeled neurons in the same regions (Figure 6A₁) (p=0.034, z-test). Nearly 75% (n = 16 of 22) of unlabeled neighboring neurons were second order with most receiving single ST inputs (Figure 6A₁). The mix of synaptic responses to second order neurons were exclusively excitatory (mono + polysynaptic) in most second order neurons whether NTS-CeA or unlabeled (Figure 6A₂). NTS-CeA second-order sensory neurons received a greater total number of ST activated synaptic inputs than unlabeled, near neighbor NTS neurons (Figure 6A₃) (Kruskal–Wallis H = 3.882 with 1 degrees of freedom. p = 0.049, one way ANOVA). Neurons lacking monosynaptic ST inputs (i.e. higher order neurons) accounted for a larger proportion of the NTS-CeA population (n = 25 of 58) and received a significantly larger proportion of synaptic inputs activated by ST shocks than unlabeled higher order neurons (n = 4 of 22, Figure 6B) (p=0.019, z-test). Thus, whether second or higher order in synaptic organization, NTS neurons projecting to the CeA received greater convergent and more complex ST-activated synaptic inputs.

Afferent information arrives sorted by TRPV1 phenotype at CeA.

Although unmyelinated (C-fiber) sensory axons constitute 75-90% of the mix of cranial visceral afferents entering NTS (Andresen *et al.*, 2012), myelinated cranial afferents dominate most regulatory reflexes which activate at physiological thresholds in the range of normal conditions (Jones & Thoren, 1977). Here we relied on TRPV1 expression as a marker of C-fiber afferents and CAP exposure to determine the myelinated/unmyelinated phenotype of the evoked antecedent ST afferent – a procedure supported by numerous previous investigations (Doyle *et al.*, 2002; Jin *et al.*, 2004). In a subset of neurons, we recruited the maximum number of ST activated synaptic inputs (Figure 7A) and then applied

CAP. CAP blocked all ST evoked transmission in neurons classified as having TRPV1+ ST inputs even at supramaximal shock intensities (Figure 7A). Neurons whose evoked transmission was unchanged by CAP were classified as belonging to TRPV1- pathways and CAP altered neither monosynaptic nor polysynaptic ST evoked EPSCs (Figure 7B). Note that all synaptic responses to CAP were all-or-none and no partial responses were detected including indirect, polysynaptic inputs to a given second order neuron (Figure 7C). If neurons had multiple ST derived inputs evident, then all ST evoked inputs were blocked by CAP in neurons with TRPV1+ primary afferents. Conversely, in TRPV1- cases, no ST evoked events were blocked during CAP regardless of whether those inputs were monosynaptic or polysynaptic or glutamatergic or GABAergic (McDougall *et al.*, 2008; McDougall & Andresen, 2012a). Such results are only consistent with a pathway organization in which the full pathway through NTS was fully segregated by the initiating TRPV1 ST phenotype. This in essence suggests a parallel pathway arrangement in which TRPV1+ ST inputs at single second order NTS neurons did not mix with TRPV1- inputs.

Afferent pathways to higher order NTS neurons remain sorted by TRPV1 ST origins.

A high proportion of NTS-CeA second-order sensory neurons received no direct ST synaptic contacts but high jitter responses indicated arrival of exclusively higher order, ST afferent information via polysynaptic pathways (Figure 8). Despite their indirect coupling to ST, these NTS-CeA higher order sensory neurons received multiple distinct inputs activated by ST afferent shocks and their organizational position deep within NTS networks with multiple inputs would seem to make them likely candidates to receive a mixed combination of TRPV1+ and TRPV1- ST afferent drive. In both labeled and unlabeled higher order neurons, introduction of CAP blocked all ST related synaptic events in half the neurons typing then as

TRPV1+ connected (Figure 8A). The remainder were unresponsive and deemed initiated by TRPV1- ST afferent axons (Figure 8B). No partial responses to CAP were detected. Together these results demonstrate that even at higher order NTS neurons and despite the presence of intervening neurons, all ST-evoked events originated from a single TRPV1 phenotypic class of ST afferents (Figure 8C). Together our results suggest that ST afferents activate pathways within NTS that are fully segregated by the initiating TRPV1 phenotype and this separation extends within the network to higher order output neurons such as those targeting CeA. The overall picture is one of parallel pathways of information sorted by the ST afferent TRPV1 phenotype. Thus, information arising from unmyelinated cranial visceral afferents is held separate throughout the NTS network from information arising from myelinated afferents.

Author Manuscript

Discussion

Stress and emotion impact the physiological state of the visceral organs and vice versa. Considerable anatomical evidence supports bidirectional neural communication between the NTS and a number of forebrain regions including the amygdala (Geerling and Loewy, 2006b), but little is understood about how ascending lines of visceral afferent communication are organized. The present studies examined this issue by retrogradely labeling NTS neurons which project to the CeA and then determined the performance of synaptic connections activated by ST cranial visceral afferents to these NTS-CeA output neurons. We report five major, new findings: 1. NTS neurons projecting to CeA were activated by ST afferent initiated pathways nearly without exception. 2. Significantly more (~half) CeA projecting NTS neurons were higher order than neighboring unlabeled neurons which were mostly (~75%) second order sensory neurons. 3. NTS-CeA neurons displayed greater numbers of convergent ST related inputs than unlabeled cells. 4. ST afferent pathways within NTS were organized into separate lines of exclusively TRPV1+ or TRPV1- viscerosensory pathways of synaptic transmission. 5. All higher order NTS neurons, whether projecting to CeA or not, received only TRPV1+ or TRPV1- ST afferent pathways despite the lack of direct ST contacts. This remarkable and absolute separation means that CeA receives a highly convergent set of craniovisceral sensory information along communication lines dedicated to one phenotypic afferent class, either TRPV1+ or TRPV1-. This TRPV1 based segregation was true whether ST information arrived in CeA after crossing a single synapse within NTS or followed multi-neuron paths within NTS which could include GABAergic interneurons. Together these findings suggest for the first time that ST afferent information courses through NTS via pathways that do not mix across TRPV1 phenotypes and resembled parallel pathways sorted by afferent phenotypic class arriving in CeA.

Visceral afferent organization within NTS delivers highly ordered information to CeA. Our results indicate that visceral organ information arrives at CeA (NTS-CeA neurons) in patterns established within NTS. Dye injected into CeA was transported retrogradely to fill neurons that were found primarily within caudal portions of medial NTS ipsilateral to the injections in CeA. This highly focused distribution within NTS corresponds to the location of the central terminal fields of a broad mix of visceral afferents such as baroreceptors, oropharyngeal afferents, airway afferents, and gastrointestinal afferents (Mendelowitz *et al.*, 1992; Sekizawa *et al.*, 2003; Rinaman & Schwartz, 2004). Previous anatomical tracing has indicated the NTS projections terminate specifically in the medial CeA (Bienkowski & Rinaman, 2013). Our results suggest that the total number of CeA projection neurons is relatively restricted and the lack of dye filled cells when injections missed their CeA target suggests a relatively delimited relationship between caudal NTS and the amygdala. These NTS-CeA neurons received strongly convergent, ST related inputs and clearly diverged from the more common pattern of neighboring second order NTS neurons which tended to receive more limited and not uncommonly single ST afferent inputs (McDougall *et al.*, 2009; Peters *et al.*, 2011; McDougall & Andresen, 2013). As unlabeled NTS second order neurons were assayed simultaneously in the same slices as NTS-CeA neurons, any systematic ST damage from slicing is unlikely to account for these differences. Thus, the high ST convergence to NTS-CeA neurons suggests that CeA receives mostly consolidated, multi-afferent signals. This high convergence is a prominent organizational feature for co-incident information processing established before reaching CeA.

The high convergence of afferent inputs at NTS-CeA neurons included polysynaptic ST-driven inputs. Polysynaptic inputs may represent a stage in the local networks within NTS with a more integrated form of sensory input. This strong tendency to receive multi-afferent ST inputs made even more surprising the absolute lack of mixing of myelinated and unmyelinated afferent messages at NTS-CeA neurons. In the physical layout within NTS, myelinated and unmyelinated ST axons branch to spread their terminal fields broadly crossing anatomical sub-regions (Kubin *et al.*, 1991; Kubin *et al.*, 2006) and cover similar areas of NTS with no discernible spatial regionalization. Despite close proximity, adjacent second order neurons received only one ST TRPV1 phenotype (McDougall & Andresen, 2013). TRPV1+ expression coincides with conduction velocities within the unmyelinated axon range and correspondingly TRPV1- afferents conducted within the A δ range (Jin *et al.*, 2004). The conformance of ST-polysynaptic inputs at NTS-CeA neurons to the TRPV1 based segregation observed in second order NTS neurons challenged our expectation that this relationship would break down deeper within the NTS local circuits to produce mixed A/C inputs at higher order neurons. The separation or organizational sorting into two streams by TRPV1 phenotype pathways appears to be generalized as it was found consistently in CeA specific projection neurons as well as unspecified neurons in the same regions (second and higher order unlabeled neurons). Polysynaptic EPSCs and IPSCs conformed to this segregation across two major neurochemical phenotypes of NTS neurons via glutamatergic and GABAergic interneurons – neither of which themselves express TRPV1 (Cavanaugh *et al.*, 2011). This surprisingly strict separation of pathway structure should provide the amygdala with cranial visceral information segregated by TRPV1 phenotype. From the perspective of the afferent sensory endings and their physiological activation characteristics (Andresen *et al.*, 2012), this phenotype sorting of myelinated and unmyelinated afferents will effectively drive two distinct pathways – the TRPV1 lacking myelinated line providing normal “physiological” status signals and the TRPV1+ or C-fiber afferents signaling potentially more

“alarming” signals. For example, during ‘rest’ it is mostly A-fiber baroreceptors that convey information to the CNS as they are activated at lower pressure (stretch) thresholds compared to C-fiber afferents (Coleridge *et al.*, 1973; Yao & Thoren, 1983). Similarly this is the case for pulmonary afferents, where at ‘rest’ A-fibers are active and at higher thresholds (greater stretch, chemical) C-fiber afferents begin to be recruited (Coleridge & Coleridge, 1984). In the gastrointestinal system it is the presence of food that stimulates release of various mediators that activate C-fiber sensory neurons, but otherwise are mostly silent (Page *et al.*, 2002). Thus, the relative roles and activation characteristics of these two classes of afferent phenotypes are systematically different in physiological contexts and in pathological states of visceral organs (Andresen *et al.*, 2012). A limitation of our approach in the present studies is that we have not identified the sensory modality (e.g. mechano- or chemo-receptor) or the visceral tissue origin (e.g. cardiac or airway) (Andresen *et al.*, 2007; Andresen & Paton, 2011; Andresen *et al.*, 2012). We do not know whether cardiac and respiratory information gets combined with gastrointestinal input through this convergence at single NTS neurons, but our studies show that they are segregated by TRPV1 phenotype. In the intact system it may be that the TRPV1- line to the CeA updates normal status but the TRPV1+ line contacts CeA neurons involved in physiological stress alarming (Dayas *et al.*, 2001). In addition, we are only considering the most direct NTS-CeA pathway here, though clearly visceral information may reach the amygdala via other intervening nuclei such as the parabrachial nucleus (Sah *et al.*, 2003). Interestingly, although our methods focused on CeA, a subset of NTS neurons projecting to the amygdala also send co-lateral axons to the periaqueductal grey (27%) (Reyes & Van Bockstaele, 2006) and to the paraventricular nucleus of the hypothalamus (10%) (Petrov *et al.*, 1993). Thus visceral information from NTS to these areas is also very likely to be similarly organized with respect to TRPV1 segregated pathways.

CeA receives highly processed visceral afferent input. Half NTS-CeA neurons were higher order and thus received ST driven local NTS network input. Our electrophysiological findings corroborates with direct synaptic function the implications from anterograde viral tracer studies in which extended infection times suggested multi-synaptic processing pathways within medial NTS before delayed expression in the amygdala following peripheral injections (Rinaman & Schwartz, 2004; McGovern *et al.*, 2012; McGovern *et al.*, 2014). Other supramedullary targets of NTS projection neurons showed highly integrative, higher order NTS neurons projecting to, for example, the paraventricular nucleus of the hypothalamus (Bailey *et al.*, 2006). In contrast, retrograde tracer injected into targets within the brainstem such as the caudal ventrolateral medulla yielded only second order NTS neurons (Bailey *et al.*, 2006). Combined, these studies illustrate how initiating visceral afferents give rise to pathway organization and this may be associated with specific efferent targets. However, little is known what these differences in afferent specificity might convey to ultimate circuit functions, e.g. single organ vs. multiple organ, high vs. low convergence or myelinated vs. unmyelinated.

NTS-CeA pathway function. The NTS-CeA pathway is well known to impact stress related behaviors with some hints about the expected general characteristics. Earlier immunohistochemical studies established that more than 50% of NTS-CeA neurons express tyrosine hydroxylase (TH) as members of the A2/C2 catecholaminergic group (Riche *et al.*, 1990; Petrov *et al.*, 1993; Reyes & Van Bockstaele, 2006). Noradrenergic NTS neurons projecting to the hypothalamus promote synaptic plasticity during stress (Inoue *et al.*, 2013) and activation of presynaptic alpha 2 receptors decrease the probability of glutamate release

from excitatory afferents in the CeA (Delaney *et al.*, 2007). During a stress response, the release of norepinephrine within the amygdala enhances memory processes (Williams *et al.*, 1998; Clayton & Williams, 2000). Subdiaphragmatic vagotomy disrupts many cranial visceral afferents although extra care is needed to maintain the health of such animals to avoid misleading results (Romanovsky *et al.*, 1997). However when carefully controlled, this surgery in rats indicates important subdiaphragmatic vagal afferent contributions to conditioned fear responses and anxiety-like behavior (Klarer *et al.*, 2014). NTS circuits participate in satiety, nausea and energy balance (Mayer, 2011; Babic & Browning, 2014) and shape behavioral responses in varying homeostatic states (Dallman, 2010), where each of these interactions may depend on NTS-CeA neurons. Combined, multi-synaptic tracing and functional studies suggest a wide range of sensory modalities reach the CeA. Our tracer identified NTS-CeA neurons were located in regions known to receive afferent inputs from multiple visceral tissues (Blessing, 1997). This fits with the idea of integrative, convergent signal processing within the NTS and thus CeA may receive a holistic view of the visceral function ranging from baroreceptors (Garfinkel *et al.*, 2014) to airway (McGovern *et al.*, 2015) and gastrointestinal vagal afferents (Viltart *et al.*, 2006). As NTS signals terminate within the medial CeA (Bienkowski & Rinaman, 2013), this information may influence or gate output activity that executes the behavioral and autonomic changes associated with fear conditioned responses (Parsons & Ressler, 2013). Indeed even at rest, the TRPV1- (A δ -fiber) line to the CeA may be influential. In support of this idea, Garfinkel *et al.* (2014) reported emotional processing and fear outcomes differed based on heartbeat such that specific fear ratings and amygdala responses (imaging) were greater during systole than in diastole.

Our most surprising finding is that myelinated visceral afferent information is strictly sorted and isolated from that of C-fibers. Our results link information processing of visceral information to the CeA and its behavioral associations. The direct NTS-CeA relationship may indicate that the amygdala has access to TRPV1-sorted information that would be essential in assessing homeostatic conditions. Information available on normal resting conditions at the visceral organs conveys a eu-physiologic signal line via the myelinated afferent driven pathways. However, the C-fibers might signal an alarming state of vulnerability or disrupted homeostasis along a dys-physiologic signal line. We speculate that these interoceptive signals affect behavioral functions via activity received along these parallel pathways from the NTS.

Author Manuscript

Translational perspective

Changes in visceral function including heart rate, breathing and digestion are concordant with emotions. We speculate that the myelinated afferent line assures “all’s well” and the C-fiber line signals “alarming” states of visceral function. The very different physiological activation profiles mean that these two parallel visceral afferent pathways encode interoceptive signals to the amygdala that may provide for homeostatic valence assessments to impact behaviors. Equally, this likely applies with external activation of the vagal afferents via vagal nerve stimulation (VNS). A-fibers exhibit electrical properties such that this subgroup is activated by VNS at the lower intensities. The upper ceiling for shock intensity in VNS devices is limited by the co-activation of vagal efferents. Our data would indicate such VNS devices likely modulate those amygdala neurons receiving A-fiber input via the NTS.

Author Manuscript

Competing interests

The authors declare no competing financial or non-financial interests.

Author contributions

SJM and MCA: conception and design of the work; SJM and HG: acquisition, analysis, or interpretation of data for the work; and all authors: drafting the work or revising it critically for important intellectual content.

Acknowledgements

Supported by grants from the National Institutes of Health; HL-41119 (MCA), HL-105703 (MCA) and Oregon Health & Science University Presidential Bridge Funding (MCA). The National Health and Medical Research Council of Australia C J Martin Fellowship #400405 (SJM) and the Victorian Government's Operational Infrastructure Support Program (Florey).

Author

REFERENCES

Acuna-Goycolea C, Brenowitz SD & Regehr WG. (2008). Active dendritic conductances dynamically regulate GABA release from thalamic interneurons. *Neuron* 57, 420-431.

Allen C & Stevens CF. (1994). An evaluation of causes for unreliability of synaptic transmission. *Proc Natl Acad Sci USA* 91, 10380-10383.

Andresen MC, Bailey TW, Jin Y-H, McDougall SJ, Peters JH & Aicher SA. (2007). Cellular heterogeneity within the solitary tract nucleus and visceral afferent processing – electrophysiological approaches to discerning pathway performance. *Tzu Chi Med J* 19, 181-185.

Andresen MC, Hofmann ME & Fawley JA. (2012). Invited Review: The un-silent majority - TRPV1 drives "spontaneous" transmission of unmyelinated primary afferents within cardiorespiratory NTS. *Am J Physiol* 303, R1207-R1216.

Andresen MC & Kunze DL. (1994). Nucleus tractus solitarius: gateway to neural circulatory control. *Ann Rev Physiol* 56, 93-116.

Andresen MC & Paton JF. (2011). The nucleus of the solitary tract: Processing information from viscerosensory afferents. In *Central Regulation of Autonomic Functions*, 2nd edn, ed: Llewellyn-Smith IJ & Verberne AJ, pp. 23-46. Oxford, London.

Andresen MC & Peters JH. (2008). Comparison of baroreceptive to other afferent synaptic transmission to the solitary tract nucleus. *Am J Physiol* 295, H2032-H2042.

Babic T & Browning KN. (2014). The role of vagal neurocircuits in the regulation of nausea and vomiting. *Eur J Pharmacol* 722, 38-47.

Bailey TW, Appleyard SM, Jin YH & Andresen MC. (2008). Organization and properties of GABAergic neurons in solitary tract nucleus (NTS). *J Neurophysiol* 99, 1712-1722.

Bailey TW, Hermes SM, Andresen MC & Aicher SA. (2006). Cranial visceral afferent pathways through the nucleus of the solitary tract to caudal ventrolateral medulla or paraventricular hypothalamus: Target-specific synaptic reliability and convergence patterns. *J Neurosci* 26, 11893-11902.

Bienkowski MS & Rinaman L. (2013). Common and distinct neural inputs to the medial central nucleus of the amygdala and anterior ventrolateral bed nucleus of stria terminalis in rats. *Brain Struct Funct* 218, 187-208.

Blessing W. (1997). *The Lower Brainstem and Bodily Homeostasis*. Oxford University Press.

Blitz DM & Regehr WG. (2005). Timing and specificity of feed-forward inhibition within the LGN. *Neuron* 45, 917-928.

Cavanaugh DJ, Chesler AT, Jackson AC, Sigal YM, Yamanaka H, Grant R, O'Donnell D, Nicoll RA, Shah NM, Julius D & Basbaum AI. (2011). Trpv1 reporter mice reveal highly restricted brain distribution and functional expression in arteriolar smooth muscle cells. *J Neurosci* 31, 5067-5077.

Clayton EC & Williams CL. (2000). Adrenergic activation of the nucleus tractus solitarius potentiates amygdala norepinephrine release and enhances retention performance in emotionally arousing and spatial memory tasks. *Behav Brain Res* 112, 151-158.

Coleridge HM, Coleridge JCG, Dangel A, Kidd C, Luck JC & Sleight P. (1973). Impulses in Slowly Conducting Vagal Fibers from Afferent Endings in the Veins, Atria, and Arteries of Dogs and Cats. *Circ Res* 33, 87-97.

Coleridge JCG & Coleridge HM. (1984). Afferent vagal C fibre innervation of the lungs and airways and its functional significance. *Rev Physiol Biochem Pharmacol* 99, 2-110.

Dallman MF. (2010). Stress-induced obesity and the emotional nervous system. *Trends Endocrinol Metab* 21, 159-165.

Danielsen EH, Magnuson DJ & Gray TS. (1989). The central amygdaloid nucleus innervation of the dorsal vagal complex in rat: a Phaseolus vulgaris leucoagglutinin lectin anterograde tracing study. *Brain Res Bull* 22, 705-715.

Dayas CV, Buller KM, Crane JW, Xu Y & Day TA. (2001). Stressor categorization: acute physical and psychological stressors elicit distinctive recruitment patterns in the amygdala and in medullary noradrenergic cell groups. *Eur J Neurosci* 14, 1143-1152.

Delaney AJ, Crane JW & Sah P. (2007). Noradrenaline modulates transmission at a central synapse by a presynaptic mechanism. *Neuron* 56, 880-892.

Doyle MW & Andresen MC. (2001). Reliability of monosynaptic transmission in brain stem neurons in vitro. *J Neurophysiol* 85, 2213-2223.

Doyle MW, Bailey TW, Jin Y-H & Andresen MC. (2002). Vanilloid receptors presynaptically modulate visceral afferent synaptic transmission in nucleus tractus solitarius. *J Neurosci* 22, 8222-8229.

Doyle MW, Bailey TW, Jin Y-H, Appleyard SM, Low MJ & Andresen MC. (2004). Strategies for cellular identification in nucleus tractus solitarius slices. *J Neurosci Meth* 37, 37-48.

Garfinkel SN & Critchley HD. (2016). Threat and the Body: How the Heart Supports Fear Processing. *Trends Cog Sci* 20, 34-46.

Garfinkel SN, Minati L, Gray MA, Seth AK, Dolan RJ & Critchley HD. (2014). Fear from the heart: sensitivity to fear stimuli depends on individual heartbeats. *J Neurosci* 34, 6573-6582.

Geerling JC & Loewy AD. (2006). Aldosterone-sensitive neurons in the nucleus of the solitary tract: bidirectional connections with the central nucleus of the amygdala. *J Comp Neurol* 497, 646-657.

Hofmann ME & Andresen MC. (2016). Vanilloids selectively sensitize thermal glutamate release from TRPV1 expressing solitary tract afferents. *Neuropharmacol* 101, 401-411.

Inoue W, Baimoukhametova DV, Fuzesi T, Cusulin JI, Koblinger K, Whelan PJ, Pittman QJ & Bains JS. (2013). Noradrenaline is a stress-associated metaplastic signal at GABA synapses. *Nat Neurosci*. 16, 605–612

Jin Y-H, Bailey TW, Li BY, Schild JH & Andresen MC. (2004). Purinergic and vanilloid receptor activation releases glutamate from separate cranial afferent terminals. *J Neurosci* 24, 4709-4717.

Jones J & Thoren PN. (1977). Characteristics of aortic baroreceptors with non-medullated afferents arising from the aortic arch of rabbits with chronic renovascular hypertension. *Acta Physiol Scand* 101, 286-293.

Kapp BS, Markgraf CG, Schwaber JS & Bilyk-Spafford T. (1989). The organization of dorsal medullary projections to the central amygdaloid nucleus and parabrachial nuclei in the rabbit. *Neurosci* 30, 717-732.

Klarer M, Arnold M, Gunther L, Winter C, Langhans W & Meyer U. (2014). Gut vagal afferents differentially modulate innate anxiety and learned fear. *J Neurosci* 34, 7067-7076.

Kubin L, Alheid GF, Zuperku EJ & McCrimmon DR. (2006). Central pathways of pulmonary and lower airway vagal afferents. *J Appl Physiol* 101, 618-627.

Kubin L, Kimura H & Davies RO. (1991). The medullary projections of afferent bronchopulmonary C fibres in the cat as shown by antidromic mapping. *J Physiol* 435, 207-228.

LeDoux JE. (2000). Emotion circuits in the brain. *Ann Rev Neurosci* 23, 155-184.

Loewy AD. (1990). Central autonomic pathways. In *Central regulation of autonomic functions*, ed. Loewy AD & Spyer KM, pp. 88-103. Oxford University Press, New York.

Maren S & Quirk GJ. (2004). Neuronal signalling of fear memory. *Nat Rev Neurosci* 5, 844-852.

Mayer EA. (2011). Gut feelings: the emerging biology of gut-brain communication. *Nat Rev Neurosci* 12, 453-466.

McDougall SJ & Andresen MC. (2012a). Low-fidelity GABA transmission within a dense excitatory network of the solitary tract nucleus. *J Physiol* 590, 5677-5689.

McDougall SJ & Andresen MC. (2012b). Low fidelity GABA transmission within a dense excitatory network of the solitary tract nucleus. *J Physiol* 590, 5677-5689.

McDougall SJ & Andresen MC. (2013). Independent transmission of convergent visceral primary afferents in the solitary tract nucleus. *J Neurophysiol* 109, 507-517.

McDougall SJ, Bailey TW, Mendelowitz D & Andresen MC. (2008). Propofol enhances both tonic and phasic inhibitory currents in second-order neurons of the solitary tract nucleus (NTS). *Neuropharmacol* 54, 552-563.

McDougall SJ, Peters JH & Andresen MC. (2009). Convergence of cranial visceral afferents within the solitary tract nucleus. *J Neurosci* 29, 12886-12895.

McGovern AE, Davis-Poynter N, Yang SK, Simmons DG, Farrell MJ & Mazzone SB. (2014). Evidence for multiple sensory circuits in the brain arising from the respiratory system: an anterograde viral tract tracing study in rodents. *Brain Struct Funct* 220, 3683-99.

McGovern AE, Driessen AK, Simmons DG, Powell J, Davis-Poynter N, Farrell MJ & Mazzone SB. (2015). Distinct brainstem and forebrain circuits receiving tracheal sensory neuron inputs revealed using a novel conditional anterograde transsynaptic viral tracing system. *J Neurosci* 35, 7041-7055.

McGovern AE, vis-Poynter N, Farrell MJ & Mazzone SB. (2012). Transneuronal tracing of airways-related sensory circuitry using herpes simplex virus 1, strain H129. *Neurosci* 207, 148-166.

Mendelowitz D, Yang M, Andresen MC & Kunze DL. (1992). Localization and retention in vitro of fluorescently labeled aortic baroreceptor terminals on neurons from the nucleus tractus solitarius. *Brain Res* 581, 339-343.

Page AJ, Martin CM & Blackshaw LA. (2002). Vagal mechanoreceptors and chemoreceptors in mouse stomach and esophagus. *J Neurophysiol* 87, 2095-2103.

Parsons RG & Ressler KJ. (2013). Implications of memory modulation for post-traumatic stress and fear disorders. *Nat Neurosci* 16, 146-153.

Pena DF, Childs JE, Willett S, Vital A, McIntyre CK & Kroener S. (2014). Vagus nerve stimulation enhances extinction of conditioned fear and modulates plasticity in the pathway from the ventromedial prefrontal cortex to the amygdala. *Front Behav Neurosci* 8, 327.

Peters JH, McDougall SJ, Fawley JA & Andresen MC. (2011). TRPV1 marks synaptic segregation of multiple convergent afferents at the rat medial solitary tract nucleus. *PLoS One* 6, e25015.

Peters JH, McDougall SJ, Fawley JA, Smith SM & Andresen MC. (2010). Primary afferent activation of thermosensitive TRPV1 triggers asynchronous glutamate release at central neurons. *Neuron* 65, 657-669.

Petrov T, Krukoff TL & Jhamandas JH. (1993). Branching projections of catecholaminergic brainstem neurons to the paraventricular hypothalamic nucleus and the central nucleus of the amygdala in the rat. *Brain Res* 609, 81-92.

Rancz EA, Ishikawa T, Duguid I, Chadderton P, Mahon S & Hausser M. (2007). High-fidelity transmission of sensory information by single cerebellar mossy fibre boutons. *Nature* 450, 1245-1248.

Reyes BA & Van Bockstaele EJ. (2006). Divergent projections of catecholaminergic neurons in the nucleus of the solitary tract to limbic forebrain and medullary autonomic brain regions. *Brain Res* 1117, 69-79.

Ricardo JA & Koh ET. (1978). Anatomical evidence of direct projections from the nucleus of the solitary tract to the hypothalamus, amygdala, and other forebrain structures in the rat. *Brain Res* 153, 1-26.

Riche D, De Pommery J & Menetrey D. (1990). Neuropeptides and catecholamines in efferent projections of the nuclei of the solitary tract in the rat. *J Comp Neurol* 293, 399-424.

Rinaman L & Schwartz G. (2004). Anterograde transneuronal viral tracing of central viscerosensory pathways in rats. *J Neurosci* 24, 2782-2786.

Romanovsky AA, Kulchitsky VA, Simons CT, Sugimoto N & Szekeley M. (1997). Febrile responsiveness of vagotomized rats is suppressed even in the absence of malnutrition. *Am J Physiol* 273, R777-783.

Sah P, Faber ES, Lopez De Armentia M & Power J. (2003). The amygdaloid complex: anatomy and physiology. *Physiological Rev* 83, 803-834.

Saper CB. (2002). The central autonomic nervous system: Conscious visceral perception and autonomic pattern generation. *Ann Rev Neurosci* 25, 433-469.

Sekizawa S, Joad JP & Bonham AC. (2003). Substance P presynaptically depresses the transmission of sensory input to bronchopulmonary neurons in the guinea pig nucleus tractus solitarii. *J Physiol* 552, 547-559.

Travagli RA, Hermann GE, Browning KN & Rogers RC. (2006). Brainstem circuits regulating gastric function. *Ann Rev Physiol* 68, 279-305.

Ulrich-Lai YM & Herman JP. (2009). Neural regulation of endocrine and autonomic stress responses. *Nat Rev Neurosci* 10, 397-409.

Viltart O, Sartor DM & Verberne AJ. (2006). Chemical stimulation of visceral afferents activates medullary neurones projecting to the central amygdala and periaqueductal grey. *Brain Res Bull* 71, 51-59.

Williams CL, Men D, Clayton EC & Gold PE. (1998). Norepinephrine release in the amygdala after systemic injection of epinephrine or escapable footshock: contribution of the nucleus of the solitary tract. *Behav Neurosci* 112, 1414-1422.

Yao T & Thoren P. (1983). Characteristics of brachiocephalic and carotid sinus baroreceptors with non-medullated afferents in rabbit. *Acta Physiologica Scand* 117, 1-8.

Author Manuscript

Figure 1. NTS projection neurons terminate at the central nucleus of the amygdala (CeA).

Cartoons depict stereotaxic placement of dye into amygdala and its retrograde transport to the caudal NTS. **A.** A coronal section that contains the terminal injection site within the left central nucleus of the amygdala (CeA) and in which the corresponding NTS contained 13 labeled neurons. Scale = 2 mm **B.** Dye injection sites are depicted overlaid onto diagrams of the nuclear divisions within the amygdala where the central nucleus is shaded red over the rostrocaudal axis relative to bregma. A total number of 442 dye-labeled NTS-CeA neurons were counted across 64 brains. The yields of back-labeled NTS projection neurons in corresponding brainstem slices is depicted by transparency levels from zero to >15 neurons per slice. Note, two additional 'zero' injections were mapped caudal of -3.14 mm bregma and are not shown. **C.** Overlay of transparency representations and plotting to NTS-CeA neuron yields relative to injections sites reveals the most consistent termination site of NTS projection neurons to the amygdala were restricted to the CeA.

Figure 2.

NTS-CeA projection and paired unlabeled neighboring neurons were distributed throughout the ipsilateral medial NTS in horizontal slices of the caudal brainstem.

Cartoons depict stereotaxic placement of dye into amygdala and its retrograde transport to the caudal NTS. **Ai & ii.** Fluorescent beads identified NTS-CeA projection neurons (green circle). **Ai & iii.** Neighboring unlabeled neurons (blue square, located more ventral in this example) were recorded alongside NTS-CeA neurons. **Aiv.** Paired recordings from medial NTS (mNTS) neurons were collected as the solitary tract was shocked with a concentric bipolar electrode (ST stim). p1 & 2, pipette 1 & 2; 4V, 4th ventricle; yellow box indicates area

depicted in panel B. **B.** NTS-CeA projection (n=58) and paired unlabeled neurons (n=22) were distributed throughout the ipsilateral medial NTS and were not observed elsewhere within any slice.

Figure 3.

NTS-CeA second-order sensory neurons receive greater convergent primary afferent input compared to unlabeled neighboring second order neurons.

NTS neurons were characterized by testing their responses to solitary tract (ST) activation using a concentric bipolar electrode. A key aspect of this assay was the pattern of synaptic response recruitment acquired by graded shock intensities used to distinguishable inputs via EPSC amplitude, synaptic jitter and failure rate. **A.** Traces from a labeled NTS-CeA second-order sensory neuron. Each panel displays ten trials overlaid (shock artifacts blanked) at increasing ST shock intensities (ST arrows). Evoked EPSCs became increasingly complex as ST shock intensities increased. Repeated shocks at 19 μ A evoked relatively low amplitude EPSCs with consistent onsets and indicate recruitment of a single input (open diamond). At 20 μ A an additional current summated with the previous, yet its onset was also very consistent, indicating recruitment of an additional input (open square). Finally, at 50 μ A an early onset EPSC was evoked and the currents summated further, indicating recruitment of a third input (open triangle). **A1.** Each of the traces in A overlaid and color coded to illustrate the EPSC dynamics with increasing shock intensities. The grey box is expanded to illustrate the differences in onset latencies. **A2.** EPSC latencies are highly consistent (low synaptic jitter) and indicate simple monosynaptic pathways from the site of axon activation (ST) to the recorded NTS-CeA projection neuron. **A3.** EPSC amplitude in relation to shock intensity illustrates the step like increments in line with all or nothing activation of afferent

inputs to NTS-CeA projection neurons. Failures (no response after ST shock) did not occur once threshold was met in this NTS-CeA second-order sensory neuron and is typical of the high probability of release from primary ST afferents. **B**. Traces from a paired unlabeled neighboring neuron where each panel displays ten trials overlaid (shock artifact blanked) at equivalent ST shock intensities (ST arrows). At 50 μA , shocks evoked low-jitter EPSCs, designating input 1 (open diamond). Each 100 μA shock triggered EPSCs with the same characteristics. Thus, super threshold shocks of any intensity successively activated the same, single, synaptic input where resultant EPSCs exhibited low jitter (**B1**, **B2**) unique threshold and zero synaptic failures (**B3**).

Figure 4.

NTS-CeA second-order sensory neurons receive convergent ST-derived polysynaptic input.

A. Traces from a labeled NTS-CeA projection neuron. Each panel displays ten trials overlaid (shock artifacts blanked) at increasing ST shock intensities (ST arrows) with the neuron held at -40 mV and -60 mV to characterize evoked IPSCs and EPSCs respectively. Repeated shocks at 16 μA evoked relatively long latency IPSCs with inconsistent onsets and failures indicating recruitment of a single polysynaptic pathway (open diamond). Shocks at 18 μA evoked an additional relatively long latency set of EPSCs also with inconsistent onsets and failures indicating recruitment of an additional excitatory polysynaptic pathway (open square). ST shocks ≥ 20 μA evoked shorter latency EPSCs with consistent onsets and no failures indicating recruitment of an additional three monosynaptic inputs (open triangle, open circle & closed hexagon). Note compound EPSC dynamics did not change beyond 35 μA (see 100 μA) indicating no additional afferent inputs were activated by ST shocks. Though disynaptic pathways are indicated in diagrams the number of intervening

interneurons per polysynaptic pathway is unknown. For an animated version of this figure please see the supplementary video. **B.** Traces in A overlaid, color coded and base levels matched to illustrate evoked EPSC and IPSC dynamics. **C.** Distribution of E & IPSC latencies illustrate long latency PSCs exhibited high jitters ($>200 \mu\text{s}$, open diamond & square) indicating complex polysynaptic pathways from the site of axon activation (ST) to the recorded NTS-CeA projection neuron. In contrast the relatively shorter latency EPSCs were more narrowly distributed and jitters $<200 \mu\text{s}$ (open triangle & circle & closed hexagon) indicating simple monosynaptic pathways from the site of axon activation (ST) to the same recorded NTS-CeA projection neuron **D.** E & IPSC amplitude in relation to shock intensity illustrates the step like increments at distinct thresholds in line with all or nothing activation of ST axons to evoke responses, note input 1 (diamonds) not plotted beyond $18 \mu\text{A}$ for clarity. Evoked E & IPSCs exhibiting high failure rates were indicative of polysynaptic pathways whereas zero failure rates were typical in low jitter EPSCs.

Figure 5.

NTS-CeA higher order sensory neurons receive convergent ST-derived polysynaptic input.

In half labeled NTS-CeA projection neurons, ST shocks activated only high jitter, polysynaptic inputs – classifying them as a higher order NTS-CeA neurons. Panels A and B display responses to ten ST shock trials overlaid (shock artifacts blanked). **A.** At $V_H = -60 \text{ mV}$, ST shocks (ST arrows) activated EPSCs with high jitter (left panel) and increases in shock intensity recruited a second, earlier arriving high jitter EPSC (right panel). **B.** In the same neuron, shifting to $V_H = -40 \text{ mV}$, $30 \mu\text{A}$ ST shocks activated outward IPSCs that did not change with higher ST shock intensities ($100 \mu\text{A}$). Note, at $V_H = -40 \text{ mV}$ inward EPSCs are also evoked as per panel A. Though disynaptic pathways are indicated in diagrams the

number of intervening interneurons per polysynaptic pathway is unknown. **C.** PSC latency distributions for all three recruited inputs were wide and exhibited high jitter indicating complex polysynaptic pathways from the site of axon activation (ST) to the recorded NTS-CeA higher order sensory neuron. **D.** PSC amplitudes increased in step-like increments, reflective of all or nothing afferent pathway activation. Failure rates for high jitter E & IPSCs were ~40% across the inputs.

Figure 6.

NTS-CeA projection neurons receive greater convergent primary and polysynaptic afferent input as compared to paired unlabeled NTS neurons.

A1. A lower proportion of NTS-CeA neurons were classified second order (receiving at least one low jitter ST input) compared to paired unlabeled neurons (50% v's 73% respectively).

A2. Within this cohort of second order NTS-CeA neurons a much greater proportion received additional polysynaptic input as compared to paired unlabeled neurons. **A3.** Second order

NTS-CeA neurons received a greater number of convergent ST afferent inputs and ST-derived polysynaptic inputs per neuron as compared to paired unlabeled neurons. Thus total

ST-derived convergence was greater too. **B.** A greater proportion of NTS-CeA neurons were classed higher order (receiving ST-derived polysynaptic input only) compared to the paired

unlabeled neuron population (43% v's 18% respectively). Within this specialized cohort NTS-CeA neurons received greater convergent polysynaptic input per neuron as compared to

paired unlabeled neurons. Note, 7% of NTS-CeA and 9% of paired unlabeled neurons were classified as 'not connected' and combined with those in A1 and B pie graphs make up the

total respective populations (NTS-CeA group n = 58, paired unlabeled group n = 22).

Figure 7.

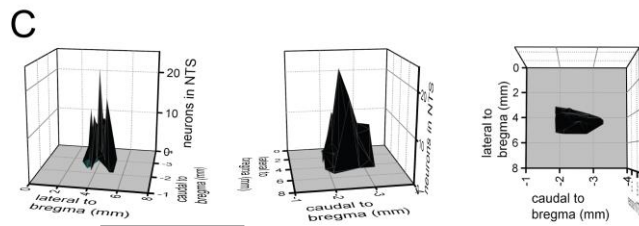
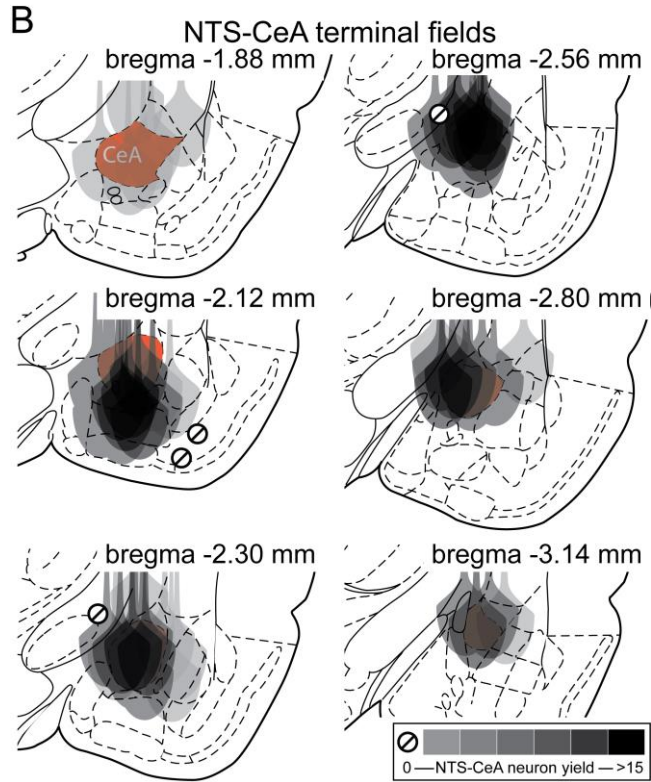
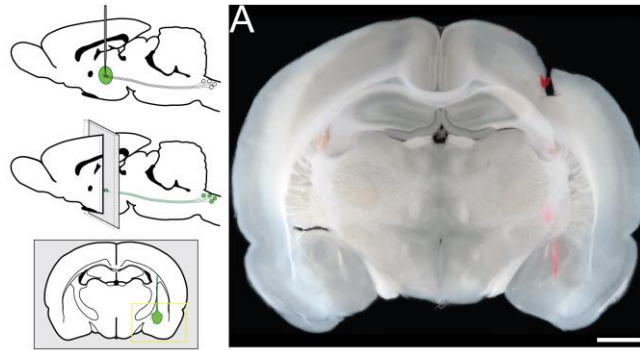
NTS-CeA second-order sensory neurons contacted by convergent monosynaptic ST afferents were either TRPV1+ or TRPV1- phenotype, never mixed.

A. Repeated increasing ST shocks (ST arrows) evoked EPSCs with consistent onsets and zero failures indicating recruitment of two monosynaptic inputs (open diamond and square) to an unlabeled NTS neuron (each panel displays ten trials overlaid, shock artifacts blanked). Shocks repeated in the presence of capsaicin (cap) were blocked indicating converging afferents both expressed TRPV1. **B.** In a NTS-CeA second-order sensory neuron repeated graded shocks (ST arrows) evoked EPSCs (ten trials overlaid, shock artifacts blanked) with consistent onsets and zero failures indicating recruitment of two monosynaptic inputs (open diamond & square) and relatively late occurring EPSCs with highly variable onsets and high failure rates indicating recruitment of an additional polysynaptic input (open triangle, not plotted in recruitment graph). Shocks repeated in the presence of capsaicin (cap) did not block these EPSCs indicating that all converging pathways (mono- as well as secondary poly-synaptic) relied on activation of primary afferents that did not express TRPV1. **C.** NTS-CeA second-order sensory and unlabeled NTS neurons received only convergent TRPV1+ (red) or – (blue) inputs, never mixed. Remarkably even polysynaptic (hashed) ST initiated events conformed to this segregation by TRPV1 phenotypic classification.

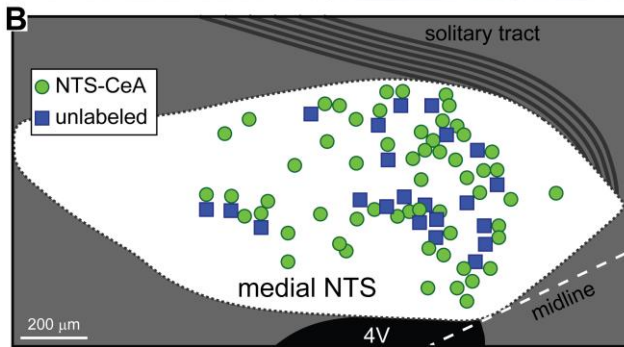
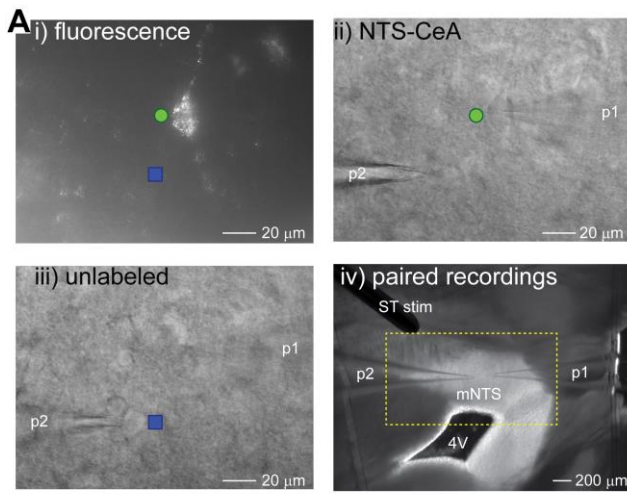
Figure 8.

Convergent ST-derived polysynaptic input to NTS-CeA higher order neurons are segregated by TRPV1 phenotype.

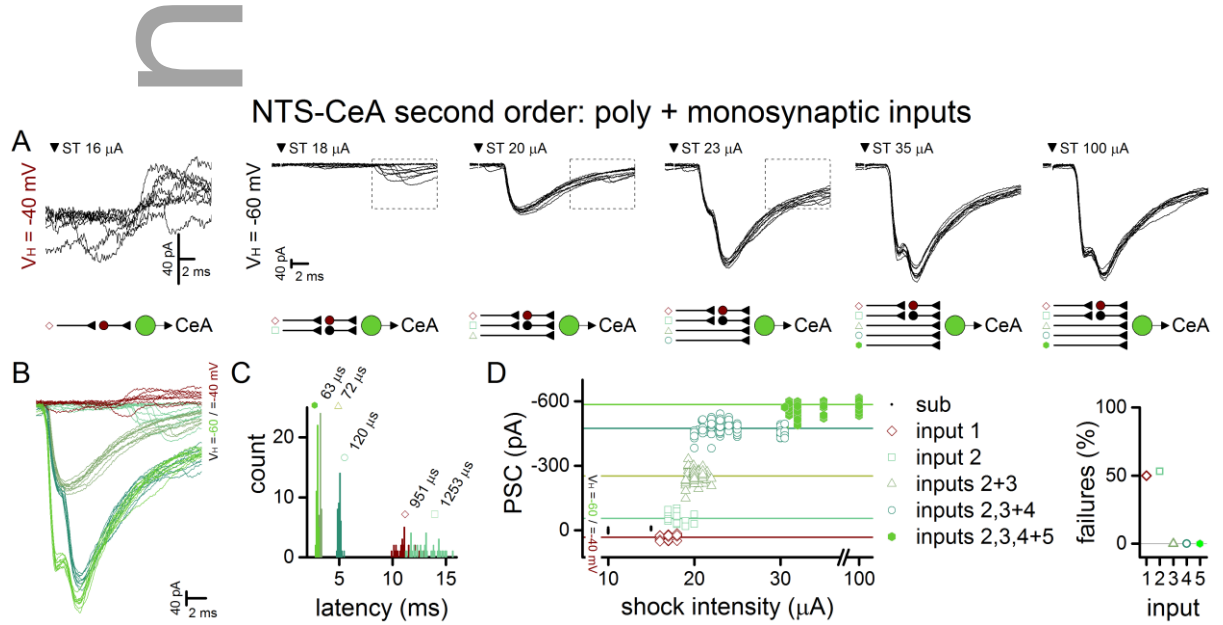
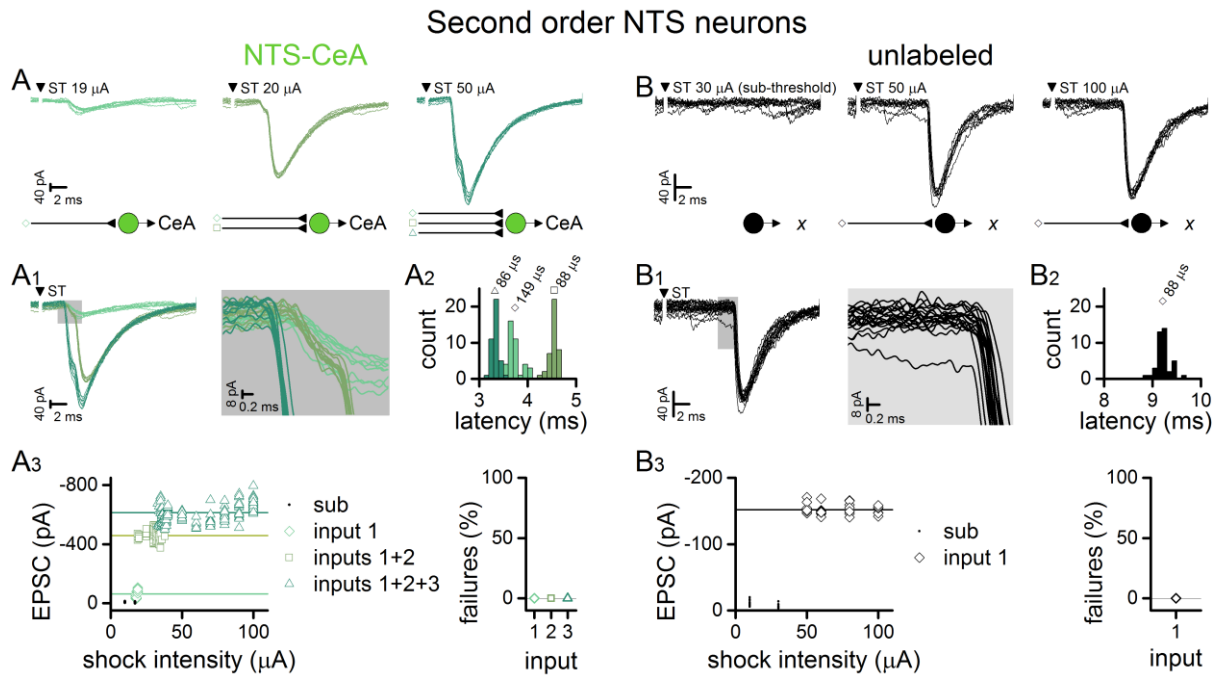
A. Repeated graded shocks evoked EPSCs (ten trials overlaid, shock artifacts blanked) with inconsistent onsets and failures indicating recruitment of two polysynaptic inputs (open diamonds & squares) to this NTS-CeA neuron. Responses to ST shocks repeated in the presence of capsaicin (cap) were blocked indicating each pathway relied on initial activation of primary afferents that expressed TRPV1. **B.** Repeated graded shocks (ST arrows) evoked EPSCs (ten trials overlaid, shock artifacts blanked) with inconsistent onsets and failures indicating recruitment of three polysynaptic inputs (open diamonds, squares & triangles) to a higher order NTS-CeA neuron. Responses to ST shocks were unaltered by capsaicin (cap) and thus were considered TRPV1- pathways. **C.** Higher order NTS neurons projecting to CeA were evenly divided by TRPV1 phenotype and on a single unlabeled higher order neuron received convergent input initiated by TRPV1+ expressing primary afferents. In all cases, converging input was segregated by TRPV1+ (red) or TRPV1- (blue) input and indicates fully segregated viscerosensory pathways within the NTS and onto the CeA.



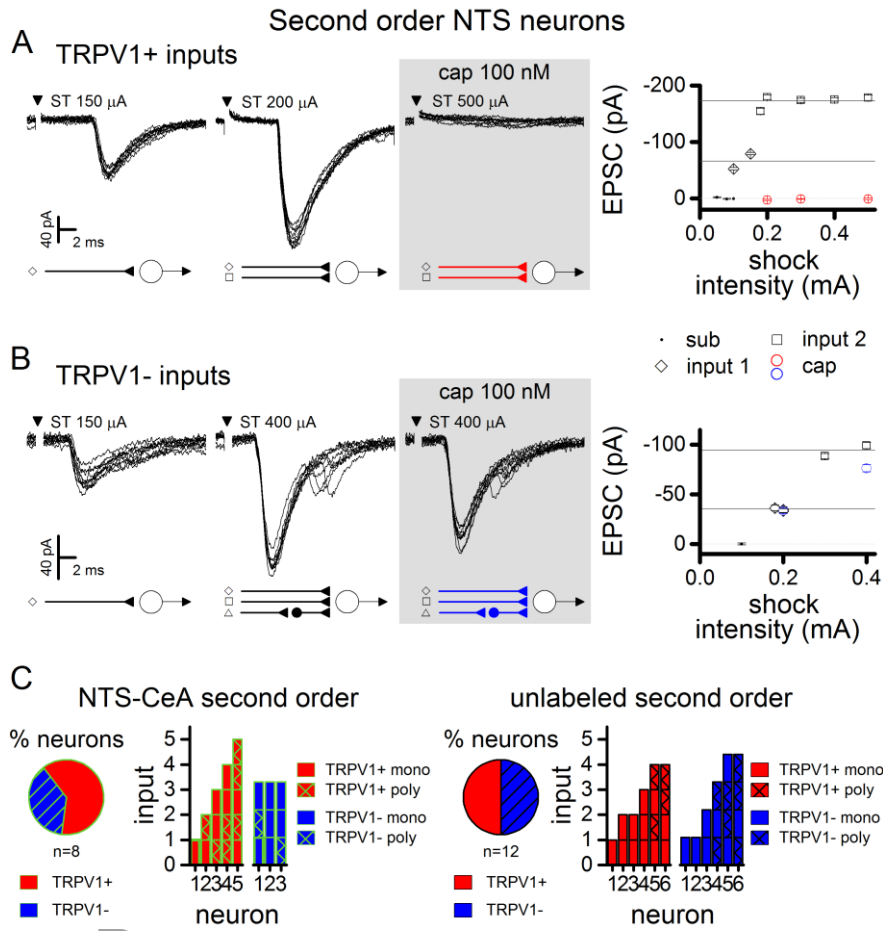
Auti



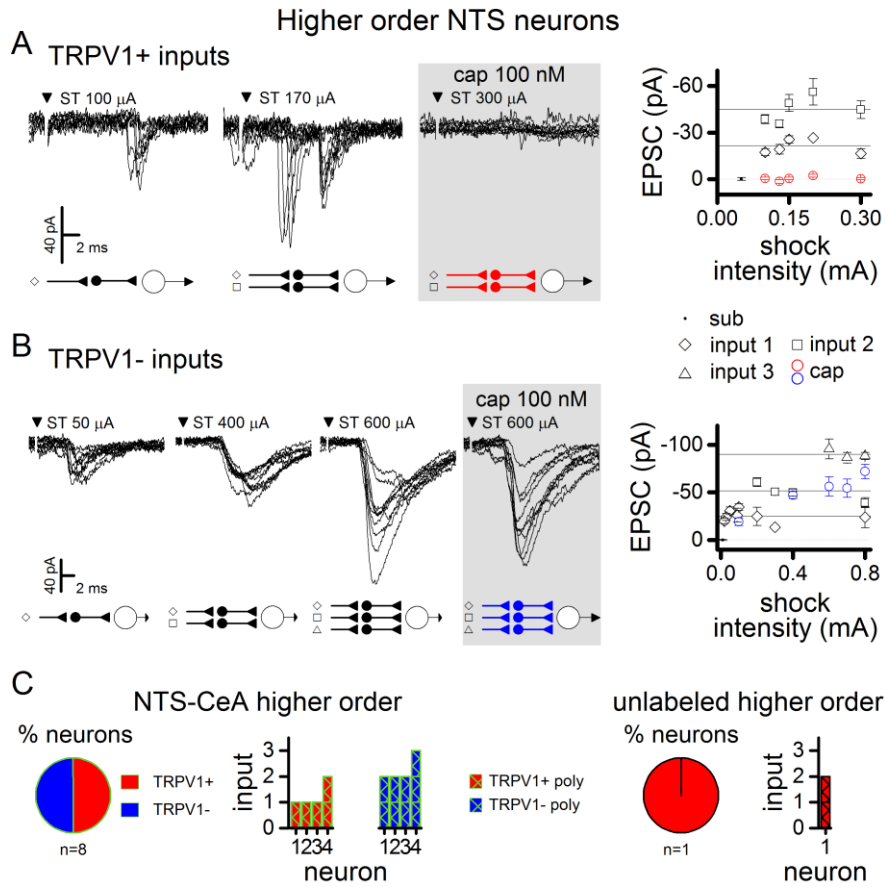
Author N



Autr



Author N



Author M